Available online at www.sciencedirect.com
SCIENCE DIRECT
Polymer 46 (2005) 5218–5224
polymer
www.elsevier.com/locate/polymer

Synthesis of polystyrene–carbon nanofibers nanocomposite foams

Jiong Shen, Changchun Zeng, L. James Lee*

Department of Chemical and Biomolecular Engineering, The Ohio State University, Columbus, OH 43210, USA

Received 9 January 2005; received in revised form 5 April 2005; accepted 6 April 2005
Available online 22 April 2005

Abstract

In this study, the use of carbon nanofibers (CNFs) as nucleating agents to produce polystyrene nanocomposite foams was demonstrated. With the addition of CNFs, microcellular foams with uniform cell size distributions were obtained. Compared to nanoclay and single-walled carbon nanotubes (SWCNTs), CNFs exhibit substantially higher nucleation efficiency in the foaming process. The underlying mechanism is semi-quantitatively explained by the classical nucleation theory. The homogeneous fiber distribution and favorable surface and geometrical characteristics of CNFs make them ideal nucleating agents.

Keywords: Carbon nanofibers; Nucleation; Microcellular foams

1. Introduction

Polymeric foams have been widely used in various applications such as cushioning, insulation, packaging and absorbency [1]. However, with the inclusion of voids into the polymer matrix, the foams usually exhibit low mechanical strength and poor dimensional stability. Recently, it has been found that microcellular foams with cell sizes less than 10 μm and cell densities larger than 10^9 cells/cm^3 hold great promise as light weight materials with excellent mechanical properties [2–7]. Small and uniform microvoids also make microcellular foams desirable as small-profile foaming parts for micro-electronic applications [8].

The production of microcellular foams usually requires a high pressure drop rate and a low foaming temperature, resulting in a very narrow operation window [9,10]. In this context, nucleating agents (nucleants) such as talc [11–13], zinc stearate [13–16], calcium carbonate [13,17], and calcium stearate [12,13,18] are used to produce microcellular foams with a high cell density and a uniform cell size distribution. More recently, nanoparticles have been studied as the foaming nucleants as well [9,19–27]. Compared to conventional micro-sized nucleants, nanoparticles offer unique advantages for controlling both the foam structures and properties. Due to the extremely small particle size, it is possible to generate a large number of nucleants with a relatively low particle loading. Furthermore, the nano-scaled dimension, the high aspect ratio, and the large surface area make those particles desirable as reinforcing elements for the cell walls.

While spherical and plate-like nanoparticles have been used to synthesize nanocomposite foams, use of cylindrical nanoparticles such as carbon nanofibers (CNFs) and single wall carbon nanotubes (SWCNTs) has not been reported. In this study, both CNFs and SWCNTs were used to synthesize polystyrene (PS) nanocomposite foams. PS nanocomposites were first prepared by means of in situ polymerization. The resulting composites were then foamed via the batch foaming process. Supercritical CO_2 was chosen as the blowing agent due to its low cost, non-toxic, non-flammable and environmentally benign properties. The nucleation efficiency of the nanoparticles is semi-qualitatively discussed using the classical nucleation theory, taking into account the nanoparticle dispersion, particle geometry and surface properties.

2. Experimental

2.1. Materials

Vapor grown carbon nanofibers (PR-24-PS, supplied by Applied Science Inc.) were pyrolytically stripped to remove

* Corresponding author. Tel.: +1 614 292 2408; fax: +1 614 292 3947.
E-mail address: lee.31@osu.edu (L.J. Lee).

0032-3861/$ - see front matter © 2005 Elsevier Ltd. All rights reserved.
doi:10.1016/j.polymer.2005.04.010

surface organic contamination. The average diameter of the CNFs was 100 nm and the original lengths ranged from 30 to 100 μm. SWCNTs (BuckyPearls™, Carbon Nanotechnologies Inc.) have an average tube diameter of 1 nm and tube length of 500 nm. Styrene and 2,2′-azobis (isobutyronitrile) (AIBN) were purchased from Aldrich and used as received.

2.2. In situ polymerization

Due to the intrinsic van der Waals attractions, SWCNTs/CNFs are tightly entangled as bundles and ropes in their original state [28–30]. Once incorporated into the polymer matrix, these attractive forces will further increase due to an entropic penalty, which is induced by the confinement of the polymer chain configuration. Therefore, the dispersion of SWCNTs/CNFs becomes a major challenge in the synthesis of polymer CNTs/CNFs composites. Strategies proposed to accomplish good dispersion include the use of ultrasonication, high shear mixing, surfactants, and functionalization of the carbon surface [28, 31–35]. In this work, we use high-shear mixing and ultrasonication to facilitate the dispersion of CNFs and SWCNTs.

Different amounts of CNFs/SWCNTs were added to the styrene monomer, together with AIBN as the initiator. The mixtures were then homogenized for 3 min and sonicated for 30 min. Polymerization was carried out isothermally at 60 °C for 20 h and the composites were post-cured at 105 °C for 2 h to complete the reaction.

2.3. Batch foaming

PS/CNFs nanocomposites were foamed with supercritical CO_2 as the blowing agent via the batch foaming process. Samples were placed in a stainless steel vessel and CO_2 was delivered via a syringe pump. The system was allowed to equilibrate at 120 °C and 13.8 MPa for 24 h. The pressure was rapidly released and the foam cells were fixed by cooling with a mixture of ice and water.

2.4. Characterization

The dispersion of nanoparticles in the polymer domain was characterized by transmission electron microscopy (TEM). Samples were microtomed at room temperature with a diamond knife and mounted on a 200-mesh copper grid. Images were obtained from a Phillips CM12 apparatus using an accelerating voltage of 80 kV. The foam morphology was characterized by scanning electron microscopy (SEM, Philips XL30). Samples were freeze-fractured in liquid nitrogen and the fracture surface was sputter-coated with gold. The resulting micrographs were analyzed by Scion Image software to determine the cell size and cell density [9]. Typically, a micrograph showing more than 50 bubbles is chosen. The number of bubbles (n) in this micrograph is determined by the software. If the area of the micrograph is A cm^2 and the magnification factor is M, the cell density (N_f) can be estimated as

$$N_f = \left(\frac{nM^2}{A}\right)^{3/2} \quad (1)$$

3. Results and discussion

3.1. PS/CNFs nanocomposite foams

A series of PS/CNFs nanocomposites with CNFs content of 0.3, 1.0, and 1.5 wt% were synthesized. These nanocomposites were subsequently foamed at 120 °C and a CO_2 pressure of 13.8 MPa. The cell morphologies are depicted in Fig. 1(a)–(c). Pure PS foam [19] (Fig. 1(f)) synthesized at the same foaming conditions is shown for comparison. In the presence of only 0.3 wt% CNFs, the cell density increased from 8.23×10^7 cells/cm^3 (pure PS foam) to 1.07×10^9 cells/cm^3, and the cell size decreased from 20 μm (pure PS foam) to 9.02 μm. By increasing the fiber content to 1 wt%, the cell density increased to 2.61×10^9 cells/cm^3 and the cell size decreased to 6.2 μm. A further increase in the CNFs content to 1.5 wt% yielded foams with the cell density of 4.59×10^9 cells/cm^3 and the cell size of 4.82 μm. All PS/CNFs foams exhibit uniform cell size distribution. These results indicate that CNFs serve well as a heterogeneous nucleating agent during the foaming process. Moreover, the monotonic increase in cell density with increasing fiber content indicates that bubble nucleation is dominated by the heterogeneous mechanism with the addition of CNFs [36].

To minimize cell interactions and cell coalescence, a sparse and stable nucleant distribution is preferred. However, we noticed that in the early stage of polymerization, the system viscosity was not high enough to achieve suitable fiber separation. Thus, the CNFs were still inclined to attract each other, causing randomly distributed aggregates up to about 1 μm in the polymer matrix, as illustrated by the TEM result (Fig. 2(a)). Although these aggregates were observed in all the composites with fiber contents from 0.3 to 1.5 wt%, only one representative TEM image (PS/1 wt% CNFs) is shown here for illustration.

In order to improve the fiber dispersion, we added 10 wt% PS into the mixture of styrene/CNFs (1 wt%) to achieve a higher initial viscosity. An extended settling time for CNFs in a more viscous medium was observed during the experiment. By increasing the AIBN content from 0.5 to 0.75 wt%, a higher rate of viscosity increase was achieved due to the increased reaction rate. As a result, the resistance force opposed to the aggregation of fibers could be increased. The ultimate fiber dispersion in the polymer is shown in Fig. 2(b). In this case, most of the fibers have been completely separated and there are no obvious fiber

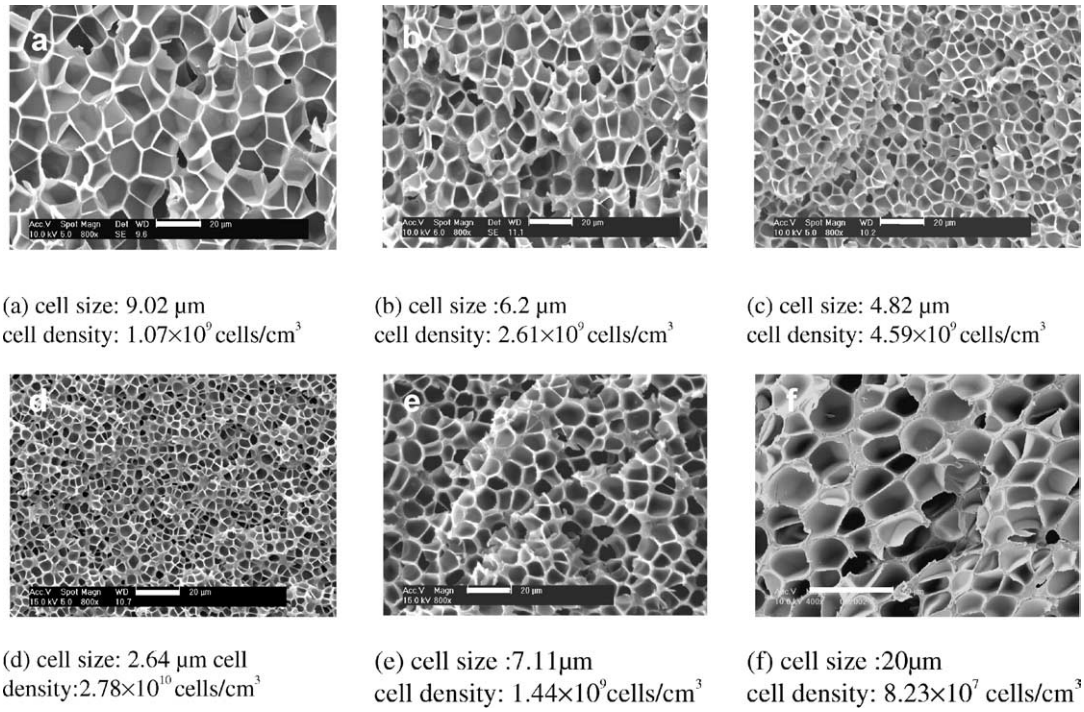

(a) cell size: 9.02 μm
cell density: 1.07×10^{9} cells/cm^3

(b) cell size :6.2 μm
cell density: 2.61×10^{9} cells/cm^3

(c) cell size: 4.82 μm
cell density: 4.59×10^{9} cells/cm^3

(d) cell size: 2.64 μm cell
density:2.78×10^{10} cells/cm^3

(e) cell size :7.11μm
cell density: 1.44×10^{9}cells/cm^3

(f) cell size :20μm
cell density: 8.23×10^{7} cells/cm^3

Fig. 1. SEM images of foams (CO_2, 13.8 MPa, 120 °C), (a–e) scale bar 20 μm (f) scale bar 50 μm (a) PS/0.3 wt% CNF, 0.5 wt% AIBN (b) PS/1 wt% CNFs, 0.5 wt% AIBN (c) PS/1.5 wt% CNFs, 0.5 wt% AIBN (d) PS/1 wt% CNFs, 0.75 wt% AIBN, 10% PS (e) PS/0.1 wt% SWCNT 0.75 wt% AIBN, 10% PS (f) pure PS [19].

aggregates, indicating a noticeable improvement of fiber dispersion. The composite was subsequently batch foamed and the foam morphology is shown in Fig. 1(d). Compared to its counterpart (Fig. 1(b)), the cell density was increased from 2.61×10^{9} to 2.78×10^{10} cells/cm^3, while the cell size decreased from 6.2 to 2.64 μm. Although the initiator concentration will influence the polymerization kinetics and eventually the molecular weight and polydispersity, a previous study showed that the effect is insignificant on the cell densities and cell sizes [37]. Hence, this dramatic change of the cell structures primarily results from the improved fiber dispersion.

3.2. PS/SWCNTs nanocomposite foams

SWCNTs were used to synthesize PS nanocomposites and foams using in situ polymerization and batch foaming processes as described previously. However, the dispersion of SWCNTs in the polymer domain is poor. From the fracture surfaces of both solid composites and foam struts, it

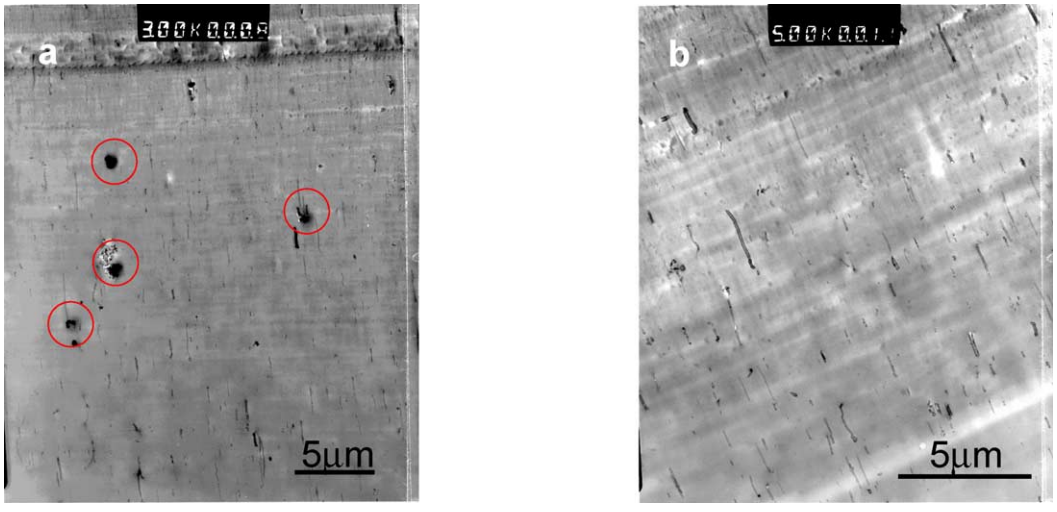

Fig. 2. TEM images of PS/CNFs nanocomposites, dark line: separated CNFs, circled particles: CNF agglomerates (a) PS/1 wt% CNFs, 0.5 wt% AIBN (b) PS/1 wt% CNFs, 0.75 wt% AIBN, 10% PS.

is very difficult to observe any dispersed SWCNT. Instead, a large amount of ball-shaped aggregates with size up to 100 nm form a bouquet-like pattern, which is similar to the fracture texture of the intercalated PS/nanoclay composite [38]. The formation of this structure could be caused by the penetration of polymer chains into the gallery of nanoparticle aggregates. For this reason, nanoparticles can be completely wrapped by the polymer, forming a large amount of ball-shaped polymer/particle agglomerates. However, even with such a poor particle dispersion, the resultant PS foam with 0.1 wt% SWCNTs still displays a much higher cell density and a much smaller cell size (Fig. 1(e)), compared to the pure PS foam. The average cell density is 1.44×10^9 cells/cm^3 and the average cell size is 7.11 μm.

3.3. Nucleation efficiencies of nanoparticles

Previously, a plate-like surface-modified nanoclay (MHABS) was also used to produce PS foams under the same conditions [9,19]. The acrylic groups attached to the clay surfaces can react with the styrene monomer, thus enabling the direct growth of polymer chains from the clay surface. Ultimately, an exfoliated dispersion of nanoclay was achieved [9]. The final PS nanocomposite foam with 5 wt% MHABS exhibited a cell density of 4.02×10^8 cells/cm^3 and an average cell size of 10.8 μm [19]. However, despite an exfoliated dispersion and a higher nominal particle loading (5 wt%), the cell density of PS/MHABS foam is still lower than any of the PS/CNFs foams attained in this study.

In heterogeneous nucleation, the highest nucleation efficiency can only be achieved when the nucleation on the nucleant surface is energetically favored (relative to its homogeneous counterpart) and the nucleant is dispersed in the polymer matrix. In most cases, the observed cell density is much lower than the potential nucleant density, implying that either the nucleants are not energetically effective, or their effects have been compromised due to poor dispersion. Here we compare the nucleation efficiencies of CNFs, SWCNTs and exfoliated nanoclay with a simple analysis.

The potential nucleant density in a heterogeneous nucleation system can be estimated by Eq. (2) [39]:

$$\frac{\text{Nucleants}}{\text{cm}^3} = \frac{w}{\rho_P}\frac{\rho_{\text{blend}}}{V_P} \tag{2}$$

where w is the weight fraction of the particle in the composite, ρ_P is the density of the particle, ρ_{blend} is the density of the polymer blend and V_P is the volume of the individual particle. In the case of CNFs, the potential nucleant density of the PS composite containing 1 wt% CNFs is 1.41×10^{12}/cm^3 according to Eq. (2). Experimentally, the cell density of the foam with the same fiber content is 2.78×10^{10} cells/cm^3 (shown in Fig. 1(d)). The proximity of these two values indicates that most of the fibers served well as nucleants in the PS foaming. The nucleation efficiency, defined by the ratio of the measured cell density to the potential nucleant density, is 1.97% for CNFs. Similar calculations were conducted for PS/MHABS and PS/SWCNTs foams and the results are listed in Table 1. For both clay and SWCNTs systems, the potential nucleant densities are much higher than the final cell densities, ultimately leading to nucleation efficiencies that are orders of magnitude lower than that of CNFs.

Based on the classical nucleation theory [16,40], the heterogeneous nucleation rate is expressed as:

$$N_{\text{het}} = \nu_{\text{het}} C_{\text{het}} \exp(-\Delta G^*_{\text{het}}/kT) \tag{3}$$

where C_{het} is the concentration of heterogeneous nucleation sites, k is the Boltzmann constant, T is the temperature, ν_{het} is the frequency factor of gas molecules merging with the nucleus, and ΔG^*_{het} is the critical Gibbs free energy to form a critical embryo on the nucleating sites, i.e.:

$$\Delta G^*_{\text{het}} = \frac{\Delta G^*_{\text{hom}}}{2} f(m,w) \tag{4}$$

$$\Delta G^*_{\text{hom}} = \frac{16\pi\gamma_{\text{lv}}}{3\Delta P^2} \tag{5}$$

$$\gamma_{\text{lv}} = \gamma_{\text{lv0}}\left[1 - \frac{T}{T_c}\right]^{11/9} \tag{6}$$

$$f(m,w) = 1 + \left(\frac{1-mw}{g}\right)^3 + w^3\left[2 - 3\left(\frac{w-m}{g}\right) + \left(\frac{w-m}{g}\right)^3\right] + 3mw^2\left(\frac{w-m}{g} - 1\right) \tag{7}$$

$$m = \cos\theta \tag{8}$$

$$w = R/r^* \tag{9}$$

$$r* = \frac{2\gamma_{\text{lv}}}{\Delta P} \tag{10}$$

$$g = (1 + w^2 - 2mw)^{1/2} \tag{11}$$

where ΔG^*_{hom} is the homogeneous Gibbs free energy, which is a function of the polymer–gas surface tension, γ_{lv}, and the pressure difference (ΔP) between that inside the critical nuclei and that around the surrounding liquid. Assuming that the polymer is fully saturated with CO_2 and the partial molar volume of CO_2 in the polymer is zero, ΔP can be taken as the difference between the saturation pressure and the atmospheric pressure [14,36]. f is the reduction of critical energy due to the inclusion of nucleants, which is a function of the polymer–gas–particle contact angle θ and the relative curvature w of the nucleant surface to the critical

Table 1
Comparison of potential nucleant density and actual cell density

Nanoparticle	wt%	Dispersion[a]	Potential nucleant density[b] (#/cm^3)	Measured cell density (#/cm^3)	Efficiency (%)
CNF	1	Complete	1.41×10^{12}	2.78×10^{10}	1.97
SWCNT	0.1	Aggregates	1.59×10^{15}	1.44×10^{9}	9.06×10^{-5}
MHABS	5	Exfoliated	5.45×10^{13}	4.02×10^{8}	7.37×10^{-4}

[a] Actual particle dispersion observed by TEM images.
[b] Calculated (Eq. (2)) with the assumption of complete particle dispersion.

radius of the nucleated phase (Eqs. (7)–(11)). r^* is the critical radius. Fig. 3 shows how the reduction of critical energy is affected by the nucleants, in terms of surface property (contact angle) and particle geometry (nucleant curvature). Qualitatively, a small contact angle and a large surface curvature offer a higher reduction of critical energy, and consequently an increased nucleation rate.

Under our foaming conditions ($T=120$ °C, $P=13.8$ MPa), γ_{lv} was calculated to be ~16.43 mJ/m^2 from Eq. (6) and the known PS–CO_2 surface tension value from the literature [41,42], r^* is 2.38 nm from Eq. (10). Thus the relative radius w is around 21 for individual CNF. With a typical contact angle of 20° [14], Eq. (7) yields a reduction factor f of 0.006 (also marked in Fig. 3), indicating that the energy required for the bubble nucleation (ΔG^*_{het}) on the surfaces of CNFs is only 0.003 ($f/2$) of that in the homogeneous case (ΔG^*_{hom}). In addition, since a complete dispersion of CNFs in the PS matrix was achieved, the actual nucleant density is close to the calculated one. The combination of the low energy barrier and the high nucleant density results in a high nucleation rate and ultimately a high cell density.

In the PS/SWCNTs system, if the SWCNTs are completely dispersed, then the relative radius w is only 0.2 considering that the radius of an individual tube is 0.5 nm. In that case, f is 1.8 and the nucleation energy on any single tube surface would approach the homogeneous limit (as shown in Fig. 3), completely diminishing the benefit of heterogeneous nucleation. However, experimentally, most SWCNTs were observed as spherical agglomerates with an average radius of approximately several dozen nanometers. These agglomerates with much larger radii can serve as lower nucleation energy sites, but the actual nucleant density is much lower than the theoretical value owing to poor dispersion, leading to the compromised nucleation efficiency.

In the PS/ MHABS system, the relatively low nucleation efficiency can be explained first by incomplete particle dispersion. Although exfoliated, stacks of multiple layers are still observable in the polymer domain [9]. A rough estimation from the TEM image of PS/5% MHANBS indicates an average stack thickness on the orders of tens of nanometers [9]. Therefore, the actual nucleant density in the PS/5% MHABS system would be reduced by one order from the value shown in Table 1, i.e. from 5.45×10^{13} to 5.45×10^{12}/cm^{-3}. This value, however, is still much higher than the measured cell density (4.02×10^{8}/cm^{-3}), suggesting that there must be other reasons accounting for the low nucleation efficiency. On the clay surface, the nucleation energy should approach to the flat plate limit ($R\rightarrow\infty$) due to the layered structure of the nanoclay. The modified clay surface is more compatible with the PS matrix, and thus the interfacial tension of the PS melt and the clay is expected to be lower than that of PS and CNFs (carbon is well known for its non-wetting property to polymers and a high polymer–particle interfacial tension). Consequently, the contact angle θ would be higher. This would lead to a significant increase in f, or much less

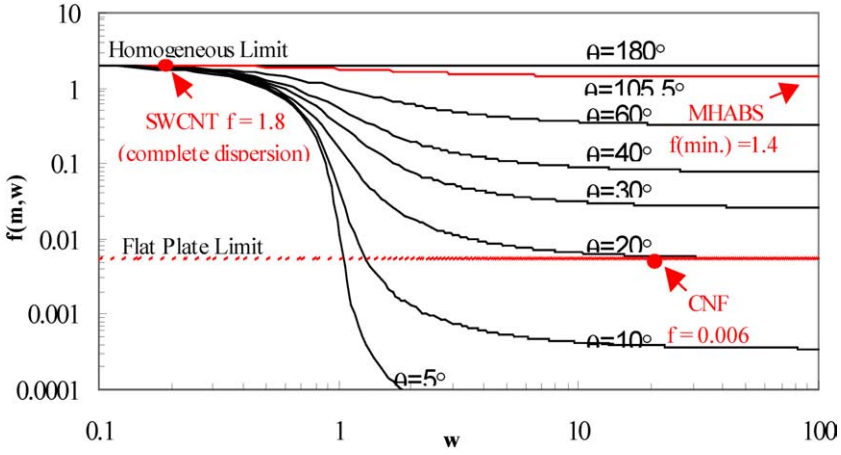

Fig. 3. Reduction of critical nucleation energy by function $f(m,w)$.

reduction of nucleation free energy. Using equilibrium interfacial tension data in the literature [43], the lower limit of θ is estimated to be 105.5° [44]. This leads to a minimum reduction factor f of 1.4 and a reduction of nucleation free energy by 30%, as illustrated in Fig. 3. Although the PS/5% MHABS system has a much higher number of potential nucleants than both the PS/1% CNFs and the PS/0.1% SWCNTs systems, its nucleation efficiency is greatly compromised by the relative ineffectiveness of the energy reduction. This analysis is in favorable agreement with the previous findings that a weak polymer particle interface is advantageous for bubble nucleation [14–16].

4. Conclusions

This study demonstrated the use of CNFs as the nucleating agents to form PS microcellular foams. It was found that the presence of a small amount of CNFs can significantly increase the cell densities and reduce the cell sizes. For comparison, SWCNTs and nanoclay were used to produce PS foams under the same foaming conditions. The nucleation efficiency, quantitatively defined as the ratio of the measured cell density to the potential nucleant density, is applied to compare the nucleation effectiveness of different particles. Based on this parameter, CNF exhibits an excellent nucleation effect on the PS foaming process. This may be due to its good dispersion in the polymer matrix, as well as the favorable wettability and surface curvature in this foaming process.

The classical nucleation theory was used to investigate the underlying mechanism for the differences in nucleation efficiencies among various particles. It was found that, with a complete dispersion and favorable particle size and surface properties, an energy reduction of 99.7% is achieved on the surfaces of CNFs. In the case of SWCNTs, the existence of the agglomerates has a mixed effect on the bubble nucleation. While the large surface radii of these agglomerates are energetically favored for the nucleation, the actual nucleant density will be greatly reduced due to the poor particle dispersion. In the case of nanoclay, an incomplete separation of the clay layers as well as the strong interactions between the clay (MHABS) surfaces and the polymer (PS) matrix lead to a deteriorated nucleation efficiency.

Acknowledgements

This work is supported by the National Science Foundation (DMI-0200324). The authors would like to thank Applied Science Inc. for donating CNFs and Dr Ben Wang at Florida A&M/Florida State University College of Engineering for providing SWCNTs. We would also like to thank Drs David L. Tomasko, Kurt W. Koelling, Xiangmin Han, Mr Maxwell Wingert and Mr Jianhua Xu at OSU for technical assistance and helpful discussions.

References

[1] Klempner D, Frisch KC. Handbook of polymeric foams and foam technology. New York: Oxford University Press; 1991.
[2] Martini-Vvedensky JE, Suh NP, Waldman FA. US Patent 4,473,665; 1984.
[3] Collias DI, Baird DG. Polym Eng Sci 1995;35:1178–83.
[4] Collias DI, Baird DG. Polym Eng Sci 1995;35:1167–77.
[5] Matuana LM, Park CB, Balatinecz JJ. Cell Polym 1998;17:1–16.
[6] Matuana LM, Park CB, Balatinecz JJ. Polym Eng Sci 1998;38: 1862–72.
[7] Seeler KA, Kumar VJ. Reinf Plast Compos 1993;12:359–76.
[8] Wang J, Cheng X, Yuan M, He J. Polymer 2001;42:8265–75.
[9] Han X, Zeng C, Lee LJ, Koelling KW, Tomasko DL. Polym Eng Sci 2003;43:1261–75.
[10] Park CB, Baldwin DF, Suh NP. Polym Eng Sci 1995;35:432–40.
[11] Park CB, Cheung LK, Song SW. Cell Polym 1998;17:221–51.
[12] Han CD, Kim YW, Malhotra KD. J Appl Polym Sci 1976;20: 1583–95.
[13] Yang HH, Han CD. J Appl Polym Sci 1984;29:4465–70.
[14] Colton JS, Suh NP. Polym Eng Sci 1987;27:485–92.
[15] Colton JS, Suh NP. Polym Eng Sci 1987;27:493–9.
[16] Colton JS, Suh NP. Polym Eng Sci 1987;27:500–3.
[17] Wilkenloh FN, Wilson PA, Fox SA. US Patent, 4,107,354; 1978.
[18] Needham DG. US Patent, 5,336,675; 1994.
[19] Zeng C, Han X, Lee LJ, Koelling KW, Tomasko DL. Adv Mater 2003; 15:1743–7.
[20] Fujimoto Y, Ray SS, Okamoto M, Ogami A, Yamada K, Ueda K. Macromol Rapid Commun 2003;24:457–61.
[21] Di Maio E, Iannace S, Di Y, Del Giacomo E, Nicolais L. Plast Rubber Compos 2003;32:313–7.
[22] Nam PH, Maiti P, Okamoto M, Kotaka T, Nakayama T, Takada M, et al. Polym Eng Sci 2002;42:1907–18.
[23] Mitsunaga M, Ito Y, Ray SS, Okamoto M, Hironako K. Macromol Mater Eng 2003;288:543–8.
[24] Ray SS, Okamoto M. Macromol Mater Eng 2003;288:936–44.
[25] Okamoto M, Nam PH, Maiti P, Kotaka T, Hasegawa N, Usuki A. Nano Lett 2001;1:295–8.
[26] Okamoto M, Nam PH, Maiti P, Kotaka T, Nakayama T, Takada M, et al. Nano Lett 2001;1:503–5.
[27] Siripurapu S, DeSimone JM, Khan SA, Spontak RJ. Adv Mater (Weinheim, Germany) 2004;16:989–94.
[28] Zhu J, Kim J, Peng H, Margrave JL, Khabashesku VN, Barrera EV. Nano Lett 2003;3:1107–13.
[29] Liao K, Li S. Appl Phys Lett 2001;79:4225–7.
[30] Qian D, Dickey EC, Andrews R, Rantell T. Appl Phys Lett 2000;76: 2868–70.
[31] Sandler J, Shaffer MSP, Prasse T, Bauhofer W, Schulte K, Windle AH. Polymer 1999;40:5967–71.
[32] Gong X, Liu J, Baskaran S, Voise RD, Young JS. Chem Mater 2000; 12:1049–52.
[33] Hill DE, Lin Y, Rao AM, Allard LF, Sun YP. Macromolecules 2002; 35:9466–71.
[34] Safadi B, Andrews R, Grulke EA. J Appl Polym Sci 2002;84:2660–9.
[35] Mitchell CA, Bahr JL, Arepalli S, Tour JM, Krishnamoorti R. Macromolecules 2002;35:8825–30.
[36] Lee ST. Foam extrusion: principles and practices. Lancaster: Technomic Publishing; 2000.
[37] Christopher CM, Russell TP, McCarthy TJ. Macromolecules 1999;32: 7610–6.
[38] Wang H. MS Thesis, The Ohio State University; 2001.

[39] Spitael P, Macosko CW, McClurg RB. Macromolecules 2004;37: 6874–82.
[40] Fletcher NH. J Chem Phys 1958;29:572–6.
[41] Wu S. Polymer interface and adhesion. New York: Marcel Dekker; 1982.
[42] Li H, Lee LJ, Tomasko DL. Ind Eng Chem Res 2004;43:509–14.
[43] Jacobasch HJ, Grundke K, Augsburg A, Gietzelt T, Schneider S. Progr Colloid Polym Sci 1997;105:44–54.
[44] Calculation of lower limit value of contact angle θ in PS/MHABS/CO_2. We have known that $\gamma_{lv}=16.43$ mJ/m^2 and $\gamma_{sl}=15$ mJ/m^2 is obtained from [43]. We need to have γ_{sv} in order to calculate θ from Young's equation $\gamma_{sl}=\gamma_{lv}\cos\theta+\gamma_{sv}$. It is known that a decrease in γ_{sv} will lead to a decrease in θ. We thus estimate the lower limit of γ_{sv} to calculate the lower limit of θ. The following three factors are considered in estimating the lower limit of γ_{sv}: (1) MHABS surface is covered by PS during nanocomposite synthesis [19]. (2) Inorganic solids have much higher γ_{sv} than organic solids like polymers. (3) For same substance, liquid has lower surface tension than solids [45]. It is therefore, reasonable to use γ_{lv} to represent the lower limit of γ_{sv}, which is 16.43 mJ/m^2. Using Young's equation, θ is calculated to be 105.5°. Higher γ_{sv} would result in higher value of θ and higher value of f.
[45] Zisman WA. Advances in chemistry series 43 (contact angle: wettability and adhesion). Washington, DC: American Chemical Society; 1964.